energies

MDPI

Article

Comparison of the Efficiency of Cross-Flow Plate Heat Exchangers Made of Varied Materials

Krzysztof Grysa, Artur Maciąg * and Artur Ściana

Faculty of Management and Computer Modelling, Kielce University of Technology, 25-314 Kielce, Poland
* Correspondence: maciag@tu.kielce.pl

Abstract: This paper discusses a mathematical model for airflow through a cross-flow plate heat exchanger. The exhaust air is used to heat the supply air. Three kinds of plates are considered: made of aluminium, copper, and steel. The purpose of this research was to verify which material used to build the plate heat exchangers uses the exhaust air heat more efficiently. The method of the Trefftz function was used to determine approximate solutions to the analysed problem. The results obtained for 1.2 mm-thick plates and for external winter, summer, and spring–autumn temperatures are discussed. The results indicate that if the efficiency and price of the metals are considered, then steel is the best material for the plate heat exchanger. Thanks to the use of thin steel plates and the reduction in air exchange time to a few minutes, a cheap and efficient cross-flow heat exchanger can be obtained.

Keywords: heat transfer; cross-flow heat exchanger; recuperator; Trefftz method

Citation: Grysa, K.; Maciąg, A.; Ściana, A. Comparison of the Efficiency of Cross-Flow Plate Heat Exchangers Made of Varied Materials. *Energies* **2022**, *15*, 8425. https://doi.org/10.3390/en15228425

Academic Editors: Tadeusz Bohdal and Marcin Kruzel

Received: 20 September 2022
Accepted: 7 November 2022
Published: 10 November 2022

1. Introduction

A recuperator is a device used, among other things, for supplying and extracting air from rooms as part of ventilation systems with heat recovery. Connected to a ventilation system, it recovers heat from the air extracted from the room, reducing the building's energy demand. The most important part of each recuperator, which determines the parameters of heat recovery, is the heat exchanger located centrally in the recuperator. There are many types of recuperators, including those discussed in monographs [1,2] and presented on many websites, including in [3]. The exhaust air flows through the heat exchanger without mixing with the supply air. Energy is exchanged between the air streams via plates that extract heat from the exhaust air and return it to the stream of fresh air. This enables the recovery of heat or cold (depending on the season). There are many publications dealing with types of heat exchangers.

Plate heat exchangers are very efficient heat transfer devices. However, their main limitation is the fact that they can only be used at a relatively low pressure and temperature [4]. Therefore, the presented article covers only the cross-flow heat exchangers operating in conditions of a small temperature difference (up to 50–60 °C) between the exhaust air and the air supplied from the outside, and discusses a mathematical model for the airflow through a cross-flow plate heat exchanger.

In our earlier paper, [5], we discussed various articles on the issues related to parallel plate heat exchangers and parallel airflow, but none of them dealt with the issue of temperature distribution in heat exchanger plates. The work [5] seems to be the first in which this issue was examined in plates of two types of exchangers depending on the material used for the plates. To the best of our knowledge, the problem of temperature distribution over time in a plate of a cross-flow exchanger has not been investigated so far.

In the cross-flow plate heat exchanger that consists of many metal plates, the heat is transferred by air streams that flow above and below them. While one section of the exchanger extracts heat from the exhaust air, the other section gives it off to the cold supply

air. This article focuses on the description of the temperature field in the cross-flow plate exchangers depending on the material from which the plates are made.

Cross-flow exchangers are used in ventilation and air-conditioning units, in systems where the following conditions are met: the separation of air streams is required; it is possible to recover energy in a reversible way; and it is possible to dry the air. The advantages of cross-flow exchangers are a lack of moving parts and electrical power, and maintenance-free operation. The disadvantages include the necessity to bring the air ducts to one place, low unit capacity, considerable overall dimensions, and high sensitivity to frost and freezing [6].

Heat exchangers are important appliances used in data centre cooling systems. In [7], the transient response of a two-dimensional, unmixed–unmixed cross-flow heat exchanger with a finite wall capacity was investigated. The concept of transient efficiency is used to build mathematical models which are used to solve and analyse transient problems with cross-flow heat exchangers. A stationary numerical model to study heat transfer in a circulating heat recovery system with two exchangers, each with a combination of counter flow and cross flow between parallel plates or membranes, is presented in [8]. The finite difference method is used to solve the equations of continuity, momentum, and steady-state heat transfer. In [9], a numerical model was developed and applied to study the fluid flow, heat, and mass transfer in a counter-cross membrane liquid–air energy exchanger (LAMEE). The iterative finite difference method is used to solve the two-dimensional steady-state flow field, and the coupled heat and moisture transfer equations for the liquid dryer and air streams. A two-dimensional, steady-state mathematical model for semi-permeable membrane-based indirect contactors as desiccants for liquid desiccant drying applications was developed in [10]. Theoretical and experimental studies of the cross-flow heat exchanger were carried out in [11] based on the theory of porous media under the low Reynolds number. The accuracy of the mathematical computational model was experimentally verified. In the study, [12], the authors investigated the operating parameters of the membrane-based parallel-plate liquid drying system. The liquid desiccant and air are in a cross pattern and are separated by semi-permeable membranes. A numerical model was developed to simulate the system's performance and was validated against experimental and analytical results.

The presented article focuses on the heat distribution in the plate of a cross-flow heat exchanger. As the plate is heated/cooled with air, the plate temperatures obtained at the inlet and outlet air correspond to the supply and exhaust air temperatures, respectively. The Fourier's law-based thermal conductivity equation is used to describe the heat flow in the plate. Boundary conditions describing the influence of air on the plate have been formulated. For the sake of simplicity, the effects related to moisture or air pollution have been omitted. Using the Trefftz method described in Section 3, approximate solutions of thermal conductivity equations for the cross-flow exchanger have been obtained and discussed.

Room temperature (21 °C) was assumed for the calculations, while the outside temperatures were simulated as follows: cold winter (−19 °C), early spring and late autumn (+1 °C), and hot summer (+31 °C). In [13], where a recuperative, counter-flow, air-to-air plate heat exchanger was numerically tested using Fluent software, it was found that it is crucial for the material to be as thin as possible so as to create the most efficient, recuperative, air-to-air heat exchanger with low pressure losses, and the properties of the material itself are not significant. In this article, plates made of three different materials are examined and the conclusions are similar.

A mathematical description of the heat transfer issues for the considered exchanger is formulated in Section 2. In Section 3, the Trefftz method is discussed. An approximation of the solution describing the initial conditions for the plate as well as an approximate solution for the transient problem have been calculated using a linear combination of Trefftz functions (T-functions). In order to find the approximate solutions, objective functionals have been built and minimized. The minimization of the functionals leads to a system of algebraic equations for the coefficients of these linear combinations. The results of the

calculations are presented in the form of graphs and tables in Section 4. In Section 5, the obtained results are discussed.

2. Formulation of Equations and Conditions for Both Tested Heat Exchangers

A heat exchanger structure is made up of subsequent plate layers separated with successive air layers, which means it is a geometrically repeatable structure (the top and bottom plates are omitted). Therefore, in the case of the "cross-flow" operation, it is sufficient to take just one plate into consideration (compare Figure 1).

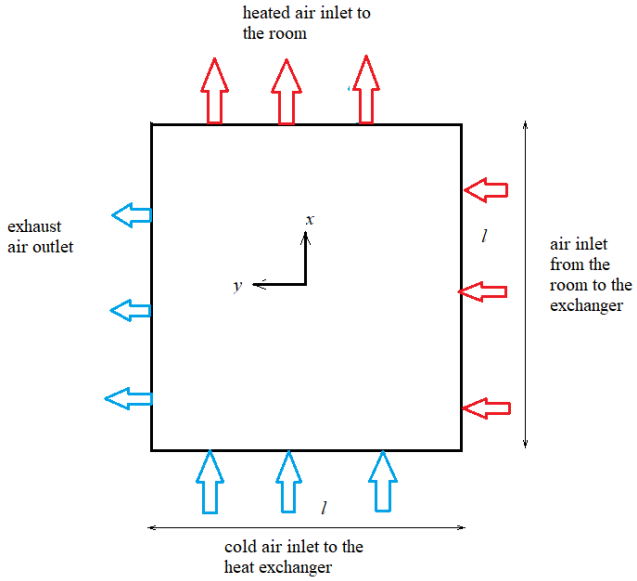

Figure 1. Cross-flow heat exchanger.

Ignoring the heat produced per unit of volume, the equation of heat conduction is obtained in the form [14,15]:

$$\nabla^2 T - \frac{1}{a}\frac{\partial T}{\partial \bar{t}} = 0 \tag{1}$$

Here, T [K] describes temperature, k [W/(mK)] describes the thermal conductivity coefficient, ρ [kg/m^3] stands for density, c [J/(kg K)] stands for specific heat, $a = \frac{k}{\rho c}\left[\frac{\mathrm{m}^2}{\mathrm{s}}\right]$ is the thermal diffusivity coefficient, $\bar{t}$ [s] stands for time, ∇ is the nabla operator and $\nabla^2 \equiv \Delta$ is the Laplace operator. Within the considered range of temperatures, the coefficients of thermal conductivity of steel, aluminium, and copper should be assumed to be constant. According to [16], the change in conductivity in the range of 200–300 K for copper is approximately (approx.) 12 W/(mK), for aluminium, the change in the conductivity value is negligible in this temperature range, and for stainless steel, it is about 2 W/(mK). According to [17], the thermal variability in conductivity in the considered temperature range for copper slowly decreases and the range of changes is about 10 W/(mK); for aluminium, it slightly increases and the changes are of the order of a few W/(mK); and in the case of stainless steel, the change is insignificant. Therefore, the assumption of constant values of conductivity in the considered temperature range seems justified.

The problem is three-dimensional. Spatial coordinates will be denoted as $\bar{x}$, $\bar{y}$, and $\bar{z}$.

The air moves between the plates at the speed of v_a [m/s]. The time of airflow between the plates is very short in relation to the total operating time of the heat exchanger; therefore, its potential influence on the thermal process is neglected.

The following dimensionless variables are introduced:

$$x = \frac{2\bar{x}}{l},\ y = \frac{2\bar{y}}{l},\ z = \frac{2\bar{z}}{l},\ Fo = \frac{a\bar{t}}{l^2} \stackrel{\text{def}}{=} t\ \text{(Fourier number)},\ Bi = \frac{\alpha l}{k}\ \text{(Biot number)} \tag{2}$$

where $\alpha \left[\frac{W}{m^2K}\right]$ is the heat transfer coefficient and $\overline{x} \in \left(\frac{-l}{2}.\frac{l}{2}\right), \overline{y} \in \left(\frac{-l}{2}.\frac{l}{2}\right), \overline{z} \in \left(\frac{-h}{2}.\frac{h}{2}\right)$, [m].

The heat transfer coefficient α will be different for the heat penetration on the side surfaces of the plate, for $\left\{(x,y,z) : x = \pm 1, y \in (-1,1), z \in \left(\frac{-h}{l}, \frac{h}{l}\right)\right\}$ or $\left\{(x,y,z) : y = \pm 1, x \in (-1,1), z \in \left(\frac{-h}{l}, \frac{h}{l}\right)\right\}$, where air is assumed to be immobile, and different on the upper and lower surfaces of the plate, $\left\{(x,y,z) : x,y \in (-1,1), z = \pm\frac{h}{l}\right\}$, where air moves at the velocity of v_a. The coefficient α is defined as falling within the range of 5 to 37 $\frac{W}{m^2K}$ [18]. The relationship between α and laminar flow velocity, v_a, is determined by the equation [19,20]:

$$\alpha = \begin{cases} 5.8 + 4v_a for v_a < 5 \text{ m/s} \\ 7.12{v_a}^2 for v_a \geq 5 \text{ m/s} \end{cases} \left[\frac{W}{m^2K}\right], \quad (3)$$

The kinematic viscosity ν for air within the range of $-20°$ to 30 °C changes in the range of 11.816 mm^2/s. For the maximum air velocity in the heat exchanger, $v_a = 4.5$ m/s, the Reynolds number $Re = v_a h/\nu$ will vary within the range of 338 to 457. This means that laminar flow occurs between the plates, since for air flowing over the flat layer (h = 0.0012 m—air duct height, adopted as plate thickness), the bottom critical Reynolds number is $Re_{kr} > 10^5$ [21–23].

On the side plate surfaces, it is assumed that air velocity is zero; i.e., the heat transfer coefficient is $\alpha_1 = 5.8$ W/(m^2K). On the upper and lower plate surfaces, $0 < v_a < 5$ m/s and $\alpha_2 = 5.8 + 4v_a$ W/(m^2K), (compare (3)). Biot numbers will be accordingly marked with Bi_1 and Bi_2.

Let us denote the temperature in the room from which the air is extracted as T_w (inside temperature) and in the outside area, as T_c (outside temperature).

First, the initial condition for the plate has to be found. The temperature distribution in the plate is then described by the following dimensionless Laplace equation

$$\nabla^2 T = 0, -1 \leq x \leq 1, -1 \leq y \leq 1, -\frac{h}{l} \leq z \leq \frac{h}{l}, \quad (4)$$

with conditions as shown in Figure 1:

$$T(x,-1,z) = T(1,y,z) = T_w - 1 \leq x \leq 1, -1 \leq y \leq 1, -\frac{h}{l} \leq z \leq \frac{h}{l}, \quad (5)$$

$$T(x,1,z) = T(-1,y,z) = T_c - 1 \leq x \leq 1, -1 \leq y \leq 1, -\frac{h}{l} \leq z \leq \frac{h}{l}. \quad (6)$$

To find the initial temperature in the plate, it is enough to solve Equation (4) with the two-dimensional Laplace operator, $\nabla^2 = \frac{\partial^2}{\partial x^2} + \frac{\partial^2}{\partial y^2}$, with an arbitrary $z \in \left(\frac{-h}{l}, \frac{h}{l}\right)$, because the plate thickness is negligible as compared to the other two dimensions. However, since the conditions (5) and (6) lead to discontinuities at points $(-1, -1, z)$ and $(1, 1, z)$, instead of them, the following conditions are adopted:

$$T(x,-1,z) = \frac{(T_c - T_w)}{32}(x-1)^4 + T_w - 1 \leq x \leq 1, -\frac{h}{l} \leq z \leq \frac{h}{l}, \quad (7)$$

$$T(1,y,z) = \frac{(T_c - T_w)}{32}(y+1)^4 + T_w - 1 \leq y \leq 1, -\frac{h}{l} \leq z \leq \frac{h}{l}, \quad (8)$$

$$T(x,1,z) = \frac{(T_w - T_c)}{32}(x+1)^4 + T_c - 1 \leq x \leq 1, -\frac{h}{l} \leq z \leq \frac{h}{l}, \quad (9)$$

$$T(-1,y,z) = \frac{(T_w - T_c)}{32}(y-1)^4 + T_c - 1 \leq y \leq 1, -\frac{h}{l} \leq z \leq \frac{h}{l}, \quad (10)$$

The heat conduction equation and conditions for $t > 0$ are as follows:

$$\nabla^2 T - \frac{\partial T}{\partial t} = 0, -1 \le x \le 1, -1 \le y \le 1, -\frac{h}{l} \le z \le \frac{h}{l}\ 0 < t \le t_{end} \tag{11}$$

with $\nabla^2 = \frac{\partial^2}{\partial \xi^2} + \frac{\partial^2}{\partial y^2} + \frac{\partial^2}{\partial z^2}$ and

$$T(x, -1, z, t) = T_w \tag{12}$$

$$\frac{\partial T(x, 1, z, t)}{\partial y} = -Bi_1[T(x, 1, z, t) - T_c] \tag{13}$$

$$\frac{\partial T(1, y, z, t)}{\partial x} = -Bi_1[T(1, y, z, t) - T_w] \tag{14}$$

$$T(-1, y, z, t) = T_c \tag{15}$$

For the air above the plate, which is to be cooled down:

$$\frac{\partial T}{\partial z}\left(x, y, \frac{h}{l}, t\right) = -Bi_2\left[T\left(x, y, \frac{h}{l}, t\right) - T_w\right], -1 \le x \le 1, -1 \le y \le 1, 0 < t \le t_{end} \tag{16}$$

For the air under the plate, which is to be heated:

$$\frac{\partial T}{\partial \zeta}\left(x, y, -\frac{h}{l}, t\right) = Bi_2\left[T\left(x, y, -\frac{h}{l}, t\right) - T_c\right], -1 \le x \le 1, -1 \le y \le 1, 0 < t \le t_{end} \tag{17}$$

3. Solution Method

3.1. Trefftz Functions

The Trefftz method, [24], will be used to solve the problem. Its purpose is in approximating the solution using a linear combination of Trefftz functions (T-functions), constructed for the Equations (4) and (11). Each of the T-functions satisfies the equation for which it has been developed.

The methods of deriving T-functions are described in many monographs and articles, including [25–27]. The authors of [28] showed that the T-function system for a linear partial differential equation is a complete system of functions. This means that any solution to this equation can be represented by an infinite series of these functions with appropriate coefficients, and a finite linear combination of these functions can be used to develop an approximate solution. Obviously, the more T-functions are used to obtain an approximate solution, the more accurate the approximation will be. In the case of the 2D T-functions for the Equation (4), these are well known and are two types of harmonic functions:

$$F_n(x, y) = \sum_{k=0}^{[n/2]} (-1)^k \frac{x^{n-2k} y^{2k}}{(n-2k)!(2k)!},\ G_n(x, y) = \sum_{k=0}^{[(n-1)/2]} (-1)^k \frac{x^{n-2k-1} y^{2k+1}}{(n-2k-1)!(2k+1)!} \tag{18}$$

for $n = 0, 1, \ldots$, with $G_0(\xi, \eta) = 0$.

T-functions for a one-dimensional problem of the form (7) read [25]:

$$v_n(x, t) = \sum_{k=0}^{[n/2]} \frac{x^{n-2k} t^k}{(n-2k)!k!} \tag{19}$$

$n = 0, 1, \ldots$ $[x]$ = floor(x) means the integer part of number x. Three-dimensional T-functions are products of one-dimensional T-functions:

$$g_m(x, y, z, t) \equiv g_{ijk}(x, y, z, t) = v_i(x, t) v_j(y, t) v_k(z, t) \tag{20}$$

with $i, j \le k, i, j, k = 0, 1, \ldots$

An approximate form of the initial condition for the plate can be written as:

$$T_M^{ap}(x, y, z) = \sum_{m=0}^{M} a_m F_m(x, y) + \sum_{m=1}^{M} b_m G_m(x, y),\ z \in \left(\frac{-h}{l}, \frac{h}{l}\right) \tag{21}$$

An approximate solution, $T_M^{ap}(\xi, \eta, \zeta, \tau)$, also expressed by dimensionless variables, (2), takes the form:

$$T_M^{ap}(x, y, z, t) = \sum_{m=0}^{M} c_m g_m(x, y, z, t) \tag{22}$$

3.2. Objective Functionals

In order to determine the constants a_m, b_m, c_m, $m = 0, 1, \ldots M$, the mean approximation of meeting the boundary conditions by the function $T_M^{ap}(x, y, z)$ (for the Equation (4)) as well as the initial and boundary conditions (for the Equation (11)) by the function $T_M^{ap}(x, y, z, t)$ will be applied. Individual conditions, (7) to (17), will be used to develop the functionals, J^{ab} and J^c, describing the inaccuracy of satisfying these conditions (so-called objective functionals). Minimization conditions for each functional will be used to derive an algebraic system of equations, at first, for the constants a_m, b_m, $m = 0, 1, \ldots M$, and then for the $\{c_m\}_{m=0,1,\ldots,M}$.

In order to find the function $T_M^{ap}(x, y, z)$, the following functional will be minimized:

$$\begin{aligned} J^{ab}(a_m, b_m) = \quad & \int_{-1}^{1} \left(\left(T_M^{ap}(x, -1, z) - \tfrac{(T_c - T_w)}{32}(x-1)^4 - T_w \right)^2 \right. \\ & \left. + \left(T_M^{ap}(x, 1, z) - \tfrac{(T_w - T_c)}{32}(x+1)^4 - T_c \right)^2 \right) dx \\ & + \int_{-1}^{1} \left(\left(T_M^{ap}(1, y, z) - \tfrac{(T_c - T_w)}{32}(y+1)^4 - T_w \right)^2 \right. \\ & \left. + \left(T_M^{ap}(-1, y, z) - \tfrac{(T_w - T_c)}{32}(y-1)^4 - T_c \right)^2 \right) dx \end{aligned} \tag{23}$$

A minimum condition for the functional $J^{ab}(a_m, b_m)$ is the zeroing of all of its first derivatives with respect to a_m and b_m, $m = 0, 1, \ldots, M$. Thus, the obtained equations form an algebraic system of 2M + 1 linear equations with 2M + 1 unknowns. They will take the form:

$$\frac{\partial J^{ab}(a_m, b_m)}{\partial a_m} = 0, m = 0, 1, \ldots, M, \ \frac{\partial J^{ab}(a_m, b_m)}{\partial b_m} = 0, m = 1, 2, \ldots, M \tag{24}$$

The solutions of the system of Equation (24) are the coefficients a_m and b_m, and consequently, the initial condition approximation $T_M^{ap}(x, y, z) \equiv T_M^{ap}(x, y, z, t = 0)$. The approximate solution of the Laplace equation, (4), contains 15 harmonic functions. For this number of functions, the error of approximation of the boundary conditions (7) to (10) does not exceed 0.005 degrees Celsius.

In order to find the function $T_M^{ap}(x, y, z, t)$, the initial and boundary conditions for the Equation (11) have to appear in the objective functional:

$$
\begin{aligned}
J^c(c_m) = \int_{-h/l}^{h/l}\int_{-1}^{1} \quad & \int_{-1}^{1}\left(T_M^{ap}(x,y,z,0) - T_M^{ap}(x,y,z)\right)^2 dxdydz \\
& + \int_0^{t_{end}}\int_{-h/l}^{h/l}\int_{-1}^{1}\left(\left(T_M^{ap}(x,-1,z,t) - T_w\right)^2\right. \\
& \left. + \left(\frac{\partial T_M^{ap}(x,1,z,t)}{\partial y} + Bi_1\left[T_M^{ap}(x,1,z,t) - T_c\right]\right)^2\right) dxdzdt \\
& + \int_0^{t_{end}}\int_{-h/l}^{h/l}\int_{-1}^{1}\left(\left(T_M^{ap}(-1,y,z,t) - T_c\right)^2\right. \\
& \left. + \left(\frac{\partial T_M^{ap}(1,y,z,t)}{\partial y} + Bi_1\left[T_M^{ap}(1,y,z,t) - T_w\right]\right)^2\right) dydzdt \\
& + \int_0^{t_{end}}\int_{-1}^{1}\int_{-1}^{1}\left(\left(\frac{\partial T_M^{ap}\left(x,y,\frac{h}{l},t\right)}{\partial z}\right.\right. \\
& \left. + Bi_2\left[T_M^{ap}\left(x,y,\frac{h}{l},t\right) - T_w\right]\right)^2 \\
& + \left(\frac{\partial T_M^{ap}\left(x,y,-\frac{h}{l},t\right)}{\partial z}\right. \\
& \left.\left. - Bi_2\left[T_M^{ap}\left(x,y,-\frac{h}{l},t\right) - T_c\right]\right)^2\right) dydzdt
\end{aligned} \tag{25}
$$

Again, a minimum condition for this functional is the zeroing of all of its first derivatives with respect to $c_m, m = 0, 1, \ldots, M$:

$$
\frac{\partial J^c(c_m)}{\partial ac_m} = 0, m = 0, 1, \ldots, M \tag{26}
$$

The solutions of the system of Equation (26) are the coefficients c_m and consequently, the approximation of the temperature field in the plate, $T_M^{ap}(x,y,z,t)$.

In order to check how many terms of the linear combination (25) have to be included in the computations to obtain a sufficient result accuracy, the values of the air outlet temperature, i.e., $T_M^{ap}(0,1,0,t_{end})$, have been checked, in cases where $M = 8, 27, 64, 125, 216 \wedge 343$ (the terms are numbered from zero). The tests adopted aluminium as the material, $\bar{t}_{end} = 300$ s as the process time, and the l and h values as in Section 4.1. For $M < 216$, the results are very inaccurate and make no physical sense due to using too few T-functions in the calculations. For $M = 216 \wedge 343$, the results presented in Table 1, calculated for three values of outside temperature T_R, exhibit slight differences at the second decimal place. For $M > 343$, the results differ from those obtained for $M = 216 \wedge 343$ at the second decimal place, but the computation time increases significantly.

Table 1. Studies involving the number of T-functions in (25) regarding computation accuracy.

Material	T_c °C	T (0,1,0,t_{end}) °C, M = 8	T (0,1,0,t_{end}), °C, M = 27	T (0,1,0,t_{end}), °C, M = 64	T (0,1,0,t_{end}), °C, M = 125	T (0,1,0,t_{end}), °C, M = 216	T (0,1,0,t_{end}) °C, M = 343
Steel $v_a = 0.5$	−19	−10.88	−5.39	−5.21	−5.93	−5.99	−5.93
	1	5.06	7.80	7.89	7.54	7.50	7.53
	31	28.97	27.60	27.55	27.73	27.75	27.73

The results of these considerations, combined with the observation that in each case, the time of calculations performed by a PC using the MAPLE program was of the order of a few minutes, finally allowed us to adopt the number of 217 T-functions, i.e., M = 216. For M = 343, the calculation time was greater than 10 min and for M = 513, almost 4 h.

4. Computation Results

The following data were adopted for the computations:

$T_w = 21$ °C (room or inside temperature),
$T_c = -19$ °C, 1 °C, or 31 °C (outside temperature),
$l = 1.2$ m (plate section length),
$h = 0.0006$ m (plate section half height),
$v_a = 0.5$ m/s and 4.5 m/s,
$\alpha_1 = 5.8 \frac{W}{m^2 K}$
$\alpha_2 = 5.8 + 4 v_a \frac{W}{m^2 K}$
$t_{end} = 300$ s,
$M = 256$ (257 T-functions).

Calculations were conducted for copper, aluminium, and steel (Table 2). The temperature of the plate was studied for $x, y \in (-1, 1), z \in \left(\frac{-h}{l}, \frac{h}{l}\right)$ and $t \in (0, t_{end})$.

Table 2. Plate material [29,30].

	ρ [kg/m^3]	c [J/(kg K)]	k [W/(mK)]	a 10^6 [m^2/s]	α (W/(m^{2}K))
Copper	8933	385	386	112.2	$5.8 + 4vv_a < 5$
Aluminium	2702	903	204	83.6	$5.8 + 4vv_a < 5$
Stainless steel	7970	561	19.5	4.36	$5.8 + 4vv_a < 5$

4.1. Results for Copper Plate

First, the copper plate was considered. The temperature distribution for the case of $T_c = -19$ °C, $v_a = 0.5$ m/s is presented in Figure 2. Graphs were obtained at $z = 0$ (because the results for $z = -h/l$ and $z = h/l$ differed by less than 0.01 °C), with dimensionless distances on the x and y axes.

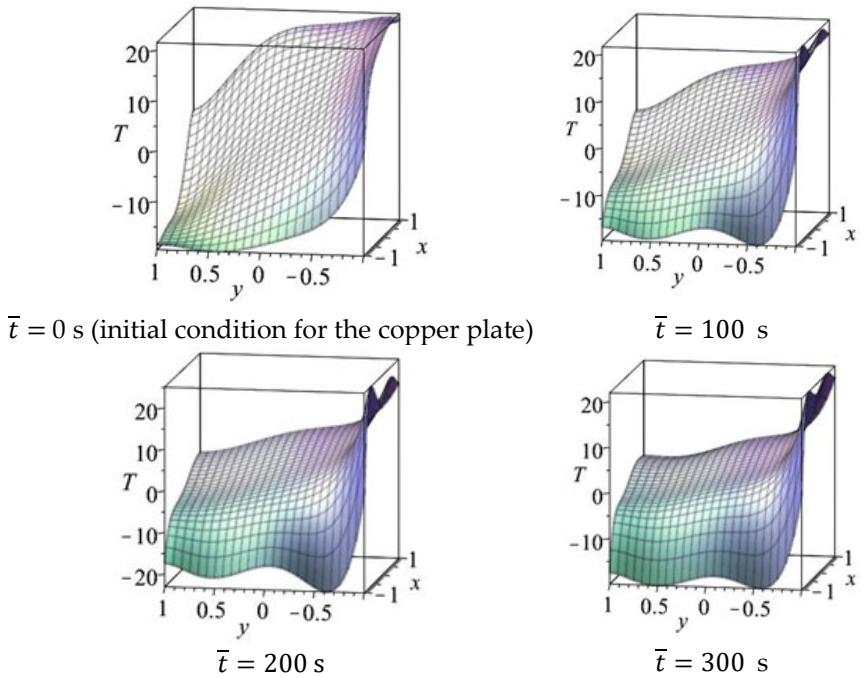

$\overline{t} = 0$ s (initial condition for the copper plate) $\overline{t} = 100$ s

$\overline{t} = 200$ s $\overline{t} = 300$ s

Figure 2. Temperature fields in the copper plate obtained at $z = 0$ and for $T_c = -19$ °C, $v_a = 0.5$ m/s, at different moments in time.

The waviness visible in the graphs results from the polynomial form of the T-function used to approximate the temperature field. Increasing the number of T-functions also

causes the truncation error to increase, and therefore, the undulations still occur (to a slightly lesser extent), but the computation time increases significantly.

It can be seen, that after just 200 s, the plate temperature stabilizes. For $\bar{t} = 300$ s, the temperature graph seems to be the least wavy. The temperatures in the corners and at the midpoint of the plate's surface facing the heated air inlet to the room for $\bar{t} = 300$ s are presented in Table 3.

Table 3. Temperatures in the corners of the copper plate and at the midpoint of the plate's surface facing the heated air inlet to the room for $T_c = -19$ °C, $v_a = 0.5$ m/s, and $\bar{t} = 300$ s.

$\bar{x}$	$l/2$	$l/2$	$-l/2$	$-l/2$	$-l/2$	$-l/2$	$l/2$	$l/2$	$l/2$	$l/2$
$\bar{y}$	$l/2$	$l/2$	$l/2$	$l/2$	$-l/2$	$-l/2$	$-l/2$	$-l/2$	0	0
$\bar{z}$	$-h/2$	$h/2$	$-h/2$	$h/2$	$-h/2$	$h/2$	$-h/2$	$h/2$	$-h/2$	$h/2$
$T^{ap}(\bar{x}, \bar{y}, \bar{z}, \mathbf{300})$ °C	1.0	1.0	−17.5	−17.5	1.0	1.0	19.5	19.5	4.5	4.5

The graphs for $v_a = 0.5$ m/s and $T_c = 1$ °C or 31 °C are of a similar nature. Therefore, for these two cases, only the temperatures at the points described in Table 3 are presented in Tables 4 and 5 below.

Table 4. Temperatures in the corners of the copper plate and at the midpoint of the plate's surface facing the heated air inlet to the room for $T_c = 1$ °C, $v_a = 0.5$ m/s, and $\bar{t} = 300$ s.

$\bar{x}$	$l/2$	$l/2$	$-l/2$	$-l/2$	$-l/2$	$-l/2$	$l/2$	$l/2$	$l/2$	$l/2$
$\bar{y}$	$l/2$	$l/2$	$l/2$	$l/2$	$-l/2$	$-l/2$	$-l/2$	$-l/2$	0	0
$\bar{z}$	$-h/2$	$h/2$	$-h/2$	$h/2$	$-h/2$	$h/2$	$-h/2$	$h/2$	$-h/2$	$h/2$
$T^{ap}(\bar{x}, \bar{y}, \bar{z}, \mathbf{300})$ °C	11.0	11.0	1.7	1.7	11.0	11.0	20.3	20.3	12.8	12.8

Table 5. Temperatures in the corners of the copper plate and at the midpoint of the plate's surface facing the heated air inlet to the room for $T_c = 31$ °C, $v_a = 0.5$ m/s, and $\bar{t} = 300$ s.

$\bar{x}$	$l/2$	$l/2$	$-l/2$	$-l/2$	$-l/2$	$-l/2$	$l/2$	$l/2$	$l/2$	$l/2$
$\bar{y}$	$l/2$	$l/2$	$l/2$	$l/2$	$-l/2$	$-l/2$	$-l/2$	$-l/2$	0	0
$\bar{z}$	$-h/2$	$h/2$	$-h/2$	$h/2$	$-h/2$	$h/2$	$-h/2$	$h/2$	$-h/2$	$h/2$
$T^{ap}(\bar{x}, \bar{y}, \bar{z}, \mathbf{300})$ °C	26.0	26.0	30.6	30.6	26.0	26.0	21.4	21.4	25.1	25.1

In Figure 3, the temperature distribution in the case of $T_c = 31$ °C and $v_a = 4.5$ m/s is presented in order to show the change in the copper plate temperature in the hot summertime. Graphs were obtained at $z = 0$.

The graphs for $v_a = 4.5$ m/s and $T_c = 1$ °C or −19 °C are of a similar nature. As for the graphs presented in Figure 2, for the time $\bar{t} = 300$ s, the temperature graph seems to be the least wavy. In all three cases, $T_c = 31$ °C, 1 °C, and −19 °C, the temperatures at the points described in Table 3 are presented below in Tables 6–8.

Table 6. Temperatures in the corners of the copper plate and at the midpoint of the plate's surface facing the inlet of heated air to the room for $T_c = 31$ °C, $v_a = 4.5$ m/s, and $\bar{t} = 300$ s.

$\bar{x}$	$l/2$	$l/2$	$-l/2$	$-l/2$	$-l/2$	$-l/2$	$l/2$	$l/2$	$l/2$	$l/2$
$\bar{y}$	$l/2$	$l/2$	$l/2$	$l/2$	$-l/2$	$-l/2$	$-l/2$	$-l/2$	0	0
$\bar{z}$	$-h/2$	$h/2$	$-h/2$	$h/2$	$-h/2$	$h/2$	$-h/2$	$h/2$	$-h/2$	$h/2$
$T^{ap}(\bar{x}, \bar{y}, \bar{z}, \mathbf{300})$ °C	26.0	26.0	30.4	30.4	26.0	26.0	21.6	21.6	26.0	26.0

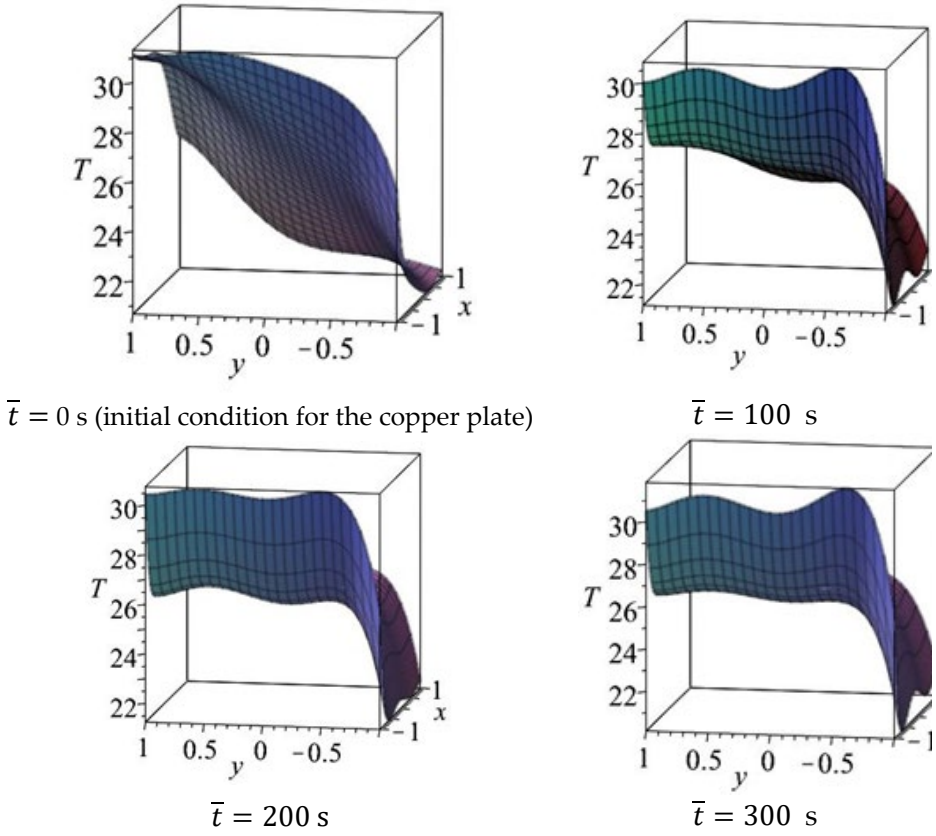

Figure 3. Temperature fields in the copper plate obtained at $z = 0$ and for $T_c = 31$ °C, $v_a = 4.5$ m/s, at different moments in time.

Table 7. Temperatures in the corners of the copper plate and at the midpoint of the plate's surface facing the heated air inlet to the room for $T_c = 1$ °C, $v_a = 4.5$ m/s, and $\overline{t} = 300$ s.

$\overline{x}$	$l/2$	$l/2$	$-l/2$	$-l/2$	$-l/2$	$-l/2$	$l/2$	$l/2$	$l/2$	$l/2$
$\overline{y}$	$l/2$	$l/2$	$l/2$	$l/2$	$-l/2$	$-l/2$	$-l/2$	$-l/2$	0	0
$\overline{z}$	$-h/2$	$h/2$	$-h/2$	$h/2$	$-h/2$	$h/2$	$-h/2$	$h/2$	$-h/2$	$h/2$
$T^{ap}(\overline{x}, \overline{y}, \overline{z}, \mathbf{300})$ °C	11.0	11.0	2.1	2.1	11.0	11.0	20.0	20.0	11.1	11.1

Table 8. Temperatures in the corners of the copper plate and at the midpoint of the plate's surface facing the heated air inlet to the room for $T_c = -19$ °C, $v_a = 4.5$ m/s, and $\overline{t} = 300$ s.

$\overline{x}$	$l/2$	$l/2$	$-l/2$	$-l/2$	$-l/2$	$-l/2$	$l/2$	$l/2$	$l/2$	$l/2$
$\overline{y}$	$l/2$	$l/2$	$l/2$	$l/2$	$-l/2$	$-l/2$	$-l/2$	$-l/2$	0	0
$\overline{z}$	$-h/2$	$h/2$	$-h/2$	$h/2$	$-h/2$	$h/2$	$-h/2$	$h/2$	$-h/2$	$h/2$
$T^{ap}(\overline{x}, \overline{y}, \overline{z}, \mathbf{300})$ °C	1.0	1.0	−16.8	−16.8	1.0	1.0	18.8	18.8	1.2	1.2

4.2. Results for a Copper, Aluminium, and Steel Plate—Comparison

The results for aluminium are similar in nature to the results for copper. This is because both metals have a very high thermal conductivity. In the case of steel, the coefficient is an order smaller, hence the graphs for steel having a different character (see the graphs presented in Figure 4 for $T_c = -19$ °C, $v_a = 0.5$ m/s); they are arranged in a manner similar to a linear distribution.

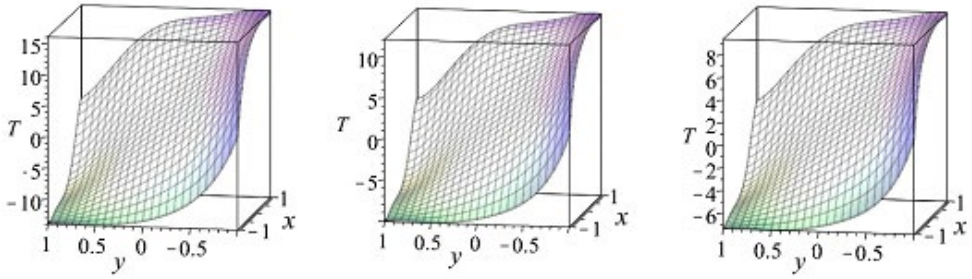

Figure 4. Temperature fields in the steel plate obtained at $z = 0$ and for $T_c = -19$ °C, $v_a = 0.5$ m/s, at different moments in time.

Tables 9–11 compare the temperatures in the corners and at the midpoint of the plate's surface facing the heated air inlet to the room, for the same temperatures at the cold air inlet, but at different air supply velocities and for different types of plates. As it follows from Table 3 to Table 8, that for $z = h/2$ and $z = -h/2$, the temperature values differ only for steel and at most by 0.1 degrees, in the following tables, the column "a" with the values of z has been omitted.

Table 9. Temperatures in the corners of different plates and at the midpoint of the plate's surface facing the heated air inlet to the room for different values of T_c, v_a, $\overline{t} = 300$ s, and $T_c = -19$ °C.

		Copper		**Aluminium**		**Steel**	
		$T_c = -19$ °C, $v_a = 0.5$ m/s	$T_c = -19$ °C, $v_a = 4.5$ m/s	$T_c = -19$ °C, $v_a = 0.5$ m/s	$T_c = -19$ °C, $v_a = 4.5$ m/s	$T_c = -19$ °C, $v_a = 0.5$ m/s	$T_c = -19$ °C, $v_a = 4.5$ m/s
$\overline{x}$	$\overline{y}$	T^{ap}	T^{ap}	T^{ap}	T^{ap}	T^{ap}	T^{ap}
$l/2$	$l/2$	1.00	1.00	1.00	1.00	1.00	1.00
$-l/2$	$l/2$	−17.50	−16.80	−17.10	−13.00	−7.40	−0.80
$-l/2$	$-l/2$	1.00	1.00	1.00	1.00	1.00	1.00
$l/2$	$-l/2$	19.50	18.80	19.10	15.00	9.39	2.80
$l/2$	0	4.50	1.20	3.30	0.90	8.00	2.40

Table 10. Temperatures in the corners of different plates and at the midpoint of the plate's surface facing the heated air inlet to the room for different values of T_c, v_a, $\overline{t} = 300$ s, and $T_c = 1$ °C.

		Copper		**Aluminium**		**Steel**	
		$T_c = 1$ °C, $v_a = 0.5$ m/s	$T_c = 1$ °C, $v_a = 4.5$ m/s	$T_c = 1$ °C, $v_a = 0.5$ m/s	$T_c = 1$ °C, $v_a = 4.5$ m/s	$T_c = 1$ °C, $v_a = 0.5$ m/s	$T_c = 1$ °C, $v_a = 4.5$ m/s
$\overline{x}$	$\overline{y}$	T^{ap}	T^{ap}	T^{ap}	T^{ap}	T^{ap}	T^{ap}
$l/2$	$l/2$	11.00	11.00	11.00	11.00	11.00	11.00
$-l/2$	$l/2$	1.70	2.10	2.00	4.00	6.81	10.10
$-l/2$	$-l/2$	11.00	11.00	11.00	11.00	11.00	11.00
$l/2$	$-l/2$	20.30	20.00	20.00	18.00	15.19	11.90
$l/2$	0	12.80	11.10	12.10	11.00	14.50	11.70

Table 11. Temperatures in the corners of different plates and at the midpoint of the plate's surface facing the heated air inlet to the room for different values of T_c, v_a, $\bar{t} = 300$ s, and $T_c = 31$ °C.

		Copper		**Aluminium**		**Steel**	
		T_c = 31°C, v_a = 0.5 m/s	**T_c = 31°C, v_a = 4.5 m/s**	**T_c = 31°C, v_a = 0.5 m/s**	**T_c = 31°C, v_a = 4.5 m/s**	**T_c = 31°C, v_a = 0.5 m/s**	**T_c = 31°C, v_a = 4.5 m/s**
$\bar{x}$	$\bar{y}$	T^{ap}	T^{ap}	T^{ap}	T^{ap}	T^{ap}	T^{ap}
$l/2$	$l/2$	26.00	26.00	26.00	26.00	26.00	26.00
$-l/2$	$l/2$	30.60	30.40	30.50	30.00	28.10	26.40
$-l/2$	$-l/2$	26.00	26.00	26.00	26.00	26.00	26.00
$l/2$	$-l/2$	21.40	21.60	21.50	22.50	23.90	25.50
$l/2$	0	25.10	26.00	25.40	26.00	24.30	25.60

Only in the case of the steel plate can one notice a difference between the temperatures of the upper and lower surfaces of the plates. This is due to the low thermal conductivity compared to other metals. In the cases of the copper and aluminium plates, the difference is smaller than 0.01 °C.

As can be seen in Tables 9–11, the temperature values at the point with the dimensional coordinates, $(l/2, 0, 0)$, lying in the centre of the side of the plate facing the heated air inlet, indicate that the exhaust air temperature, cooled by the incoming fresh air, strongly cools the air entering the room. At the velocity $v_a = 0.5$ m/s of both air streams (above and below the plate), the temperature values achieved at this point are much closer to the temperature of 21 °C than at the velocity $v_a = 4.5$ m/s. Thus, the cross-flow heat exchanger should be operated at low airflow velocities.

5. Discussion

Following Saint-Venant's principle, the temperature charts after 300 s practically do not depend on the type of conditions adopted for the initial moment. The conditions that have been tested describe a constant temperature at the plate sides with discontinuity at two corner points, with temperature changing linearly from T_c or T_w to mean temperatures at these corners, and changing like a 4th degree parabola (formulas (7) to (10) adopted in this article for calculations). The temperature distribution in the slab for each of the three mentioned initial conditions at the copper plate sides is shown in Figure 5.

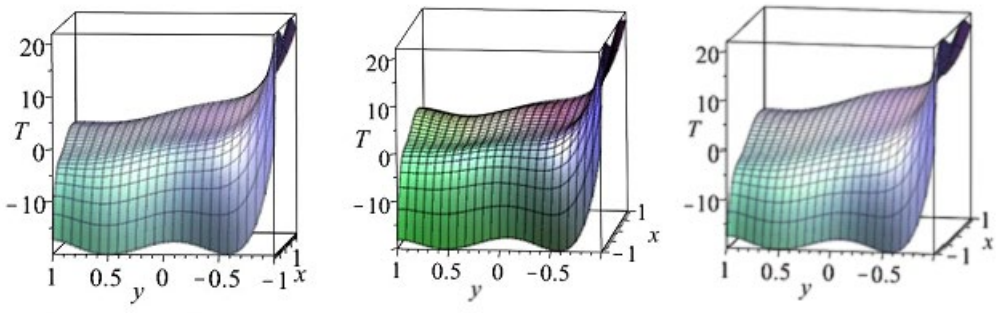

Figure 5. Temperature fields in the copper plate obtained at t = 300 s and for $T_c = -19$ °C, $v_a = 0.5$ m/s, for the initial conditions changing linearly, remaining constant, and changing like a 4th degree parabola, respectively.

The temperature values in the corners and at the point $(l/2, 0, 0)$ for the results obtained for these three types of initial conditions for the copper plate are shown in Table 12. At the point, $(l/2, 0, 0)$, the difference between the temperature values is the greatest. In the corners, it does not exceed 1 degree.

Table 12. Temperatures in the corners of the copper plate and at the midpoint of the plate's surface facing the heated air inlet to the room for different initial conditions, and $v_a = 0.5$ m/s, $T_c = -19$ °C, and $\bar{t} = 300$ s.

$\bar{x}$	$\bar{y}$	T (lin)	T (const)	T (parab)
$l/2$	$l/2$	1.01	1.00	1.00
$-l/2$	$l/2$	−17.50	−18.30	−17.50
$-l/2$	$-l/2$	0.53	1.00	1.00
$l/2$	$-l/2$	20.10	20.30	19.50
$l/2$	0	3.80	1.83	4.50

It is worth noting how the cross-flow heat exchanger behaves when the plate is twice as thin as the one adopted for this article. An aluminium plate was used for the tests. The presented research shows that the thinner the plate, the less the supply air heats up, although the differences are small. The differences in the final air temperatures are a bit closer to 21 °C (room temperature) at the point $(-l/2, l/2, 0)$ when $T_c = -19$ °C and $T_c = 1$ °C, as shown in Table 13. At the points $(l/2, l/2, 0)$ and $(-l/2, -l/2, 0)$, the values of the temperature are equal for both assumed values of plate thickness. At $(l/2, -l/2, 0)$ (inlet of the exhaust air from the room), the temperature values are closer to 21 °C (room temperature) for $h = 0.0012$ m. Similar results were obtained for a steel plate (Table 14).

Table 13. Comparison of the temperatures in the corners of a plate and at the midpoint of the plate's surface facing the heated air inlet to the room made of 0.0012 m and 0.0006 thick aluminium plates, for an air exchange duration of $t_{end} = 300$ s, and air velocities of v_a = 0.5 m/s and v_a = 4.5 m/s.

T [°C]		−19	−19	1	1	31	31	−19	−19	1	1	31	31
v_a **[m/s]**		0.5	4.5	0.5	4.5	0.5	4.5	0.5	4.5	0.5	4.5	0.5	4.5
$\bar{x}$	$\bar{y}$			$h = 0.0006$ m						$h = 0.0012$ m			
$l/2$	$l/2$	1.0	1.0	11.0	11.0	26.0	26.0	1.0	1.0	11.0	11.0	26.0	26.0
$-l/2$	$l/2$	−15.8	−8.9	2.6	6.0	30.2	28.5	−17.1	−13.0	2.0	4.0	30.5	30.0
$-l/2$	$-l/2$	1.0	1.0	11.0	11.0	26.0	26.0	1.0	1.0	11.0	11.0	26.0	26.0
$l/2$	$-l/2$	17.8	10.9	19.4	16.0	21.8	23.5	19.1	15.0	20.0	18.0	21.5	22.5
$l/2$	0	1.3	1.4	11.2	11.2	25.9	25.9	3.3	0.9	12.1	11.0	25.4	26.0

Table 14. Comparison of the temperatures in the corners of a plate and at the midpoint of the plate's surface facing the heated air inlet to the room, made of 0.0012 m and 0.0006 thick steel plates, for an air exchange duration of $t_{end} = 300$ s, and air velocities of v_a = 0.5 m/s and v_a = 4.5 m/s.

T [°C]		−19	−19	1	1	31	31	−19	−19	1	1	31	31
v_a **[m/s]**		0.5	4.5	0.5	4.5	0.5	4.5	0.5	4.5	0.5	4.5	0.5	4.5
$\bar{x}$	$\bar{y}$			$h = 0.0006$ m						$h = 0.0012$ m			
$l/2$	$l/2$	1.00	1.00	11.00	11.00	26.00	26.00	1.00	1.00	11.00	11.00	26.00	26.00
$-l/2$	$l/2$	−3.10	0.10	8.90	10.60	27.00	26.20	−7.40	−0.80	6.81	10.10	28.10	26.40
$-l/2$	$-l/2$	1.00	1.00	11.00	11.00	26.00	26.00	1.00	1.00	11.00	11.00	26.00	26.00
$l/2$	$-l/2$	5.10	1.90	13.10	11.40	25.00	25.80	9.39	2.80	15.19	11.90	23.90	25.50
$l/2$	0	4.10	1.80	12.60	11.40	25.00	25.80	8.00	2.40	14.50	11.70	24.30	25.60

Consider the temperature transfer efficiency of copper, aluminium, and steel cross-flow heat exchangers. The efficiency of the heat exchanger, understood as the efficiency of

heat exchange during the flow of the working medium through the exchanger, is the ratio of the output of useful energy exchange to the total input of heat energy exchange. The efficiency is calculated from the formula [31]:

$$\eta_T = \frac{T_{\text{in}} - T_c}{T_w - T_c}$$

As AAs T_{in}, half of the sum of T_w, and the average temperature of the heated air entering the room is taken. The latter is calculated as the integral with respect to $\overline{y}$ of the temperature $T^{ap}(l/2, \overline{y}, 0)$, divided by l. The values of T_{in} and the efficiency η_T for the three considered cross-flow heat exchangers for different values of T_c and v_a, and for $h = 0.0012$ m, for aluminium, are presented in Table 15.

Table 15. Comparison of the efficiency of plates of the thickness $h = 0.0012$ m made of copper, aluminium, and steel for an air exchange duration of $t_{end} = 300$ s, and air velocities of v_a = 0.5 m/s and v_a = 4.5 m/s.

T [°C]	−19	−19	1	1	31	31	−19	−19	1	1	31	31
v_a [m/s]	0.5	4.5	0.5	4.5	0.5	4.5	0.5	4.5	0.5	4.5	0.5	4.5
Plate made of	η_T						T_{in}					
Cu	0.80	0.76	0.80	0.76	0.80	0.76	13.01	11.29	17.01	16.15	23.00	23.43
Al	0.78	0.75	0.78	0.75	0.78	0.75	12.30	10.93	16.65	15.96	23.18	23.52
Steel	0.82	0.77	0.82	0.77	0.82	0.77	13.93	11.61	17.46	16.31	22.77	23.35

The highest efficiency values were obtained for the steel plates. The efficiency values for the copper plates are slightly higher than for the aluminium plates. However, copper is more expensive than aluminium and steel (steel is \$2.02/lb, aluminium is \$2.79/lb, while copper is \$3.52/lb, [32,33]), and is therefore omitted in further discussion concerning the exhaust-supply heat exchanger. The steel heat exchanger is also the cheapest. The efficiency values for aluminium plate heat exchangers for $h = 0.0006$ m for both velocities are practically the same (i.e., $\eta_{T,Al} = 0.75$), as for $h = 0.0012$ m and $v_a = 4.5$ m/s. For 0.0006 m-thick steel plates, the efficiency values are $\eta_{T,Steel} = 0.78$ for $v_a = 0.5$ m/s and $\eta_{T,Steel} = 0.76$ for $v_a = 4.5$ m/s. This means that steel cross-flow exchangers, even with thin plates, have almost the same efficiency as the copper and aluminium exchangers described above, and at the same time, they are cheaper. In addition, the use of thinner steel plates can reduce the weight of the exchanger.

6. Conclusions

Trefftz functions were adopted as the baseline for the approximate solution to the problem. According to our knowledge, this article is one of the first in which the approximation of the solution by three-dimensional time-dependent T-functions was used. As shown in Table 1, in order to obtain an approximate solution with an accuracy of 0.1 degrees Celsius, at least the first 217 T-functions must be considered. However, even for this seemingly large number of functions, the boundary conditions are met with an accuracy of a few degrees, and the solution itself, even after 300 s, shows some undulations. This is related to the necessity to approximate the constant values of temperature at the two boundaries of the plate, which is only possible to obtain with the use of polynomial T-functions when using a very large number of functions, in the order of thousands. However, in that case, the computing time on a PC is unacceptable. While with 217 functions, the calculation time for one variant (metal, temperatures T_c and T_w, time from 0 to 300 s, selected air flow velocity above/below the plate) was several minutes, increasing the number of functions to 513 was associated with many hours of calculations. This is related to the need to solve big systems of linear equations in order to obtain the coefficients of linear combinations of T-functions, describing an approximate solution.

As could be expected, the plate thickness (1.2 mm) in relation to the other two dimensions means that although the heat conduction equation was solved for x, y, z, and t, the results practically depend only on x, y, and t. It follows that the plate section of the heat exchanger can be considered two-dimensional.

The results clearly show how temperature distribution depends on air velocity. Increasing the velocity of the air stream above/below the plate reduces the heating of the air flowing from the environment to the room. The higher the air velocity in the exchanger, the shorter the residence time above/below the separating plate. For the velocity of 0.5 m/s, the residence time above/below the plate is 2 s; for the velocity of 4.5 m/s it is 0.22 s. In a shorter amount of time, the air will not have time to heat up more than when it flows at a lower speed, because then, the amount of time for taking up/releasing heat is longer. In numerical terms, this is described in Tables 9–11. This means that in practice, the cross-flow heat exchangers should operate at a low air stream velocity v_a.

It is worth mentioning that the proposed methodology was partially validated. Namely, the temperature was measured at the inlet of cold air to the heat exchanger with aluminium plates and at the outlet of heated air to the room. The measurements were made in the temperature range of 10 to 31 °C at the air flow velocity of about 0.86 m/s. For this flow rate, the temperature at the outlet differs only slightly from the one obtained at 0.5 m/s. For an ambient temperature of 10 °C, a temperature of 21.5 °C was obtained at the inlet to the room. For an ambient temperature of 31 °C at the inlet to the room, it was 21.7 °C. Tables 10 and 11 show the temperature at the point $\left(\frac{l}{2}, -\frac{l}{2}, \mp\frac{h}{2}\right)$ for the ambient temperatures of 1 °C and 31 °C for the aluminium plate and at an air velocity of 0.5 m/s. This temperature for the ambient temperature T_c = 1 °C is equal to 20 °C and is slightly lower than that measured for T_c = 10 °C, which is reasonable. For T_c = 31 °C, the calculated temperature is 21.5 °C and differs slightly from the measured temperature. The measurements were taken at the Energent Polska production plants in Kielce, Poland.

Reducing the plate thickness from 1.2 mm to 0.6 mm slightly reduced the efficiency of the exchanger (compare the results presented in Table 15 and the comments under this table concerning thin aluminium and steel plates). Because at the same time it turned out that exchangers with steel plates are the most effective, and as such have the lowest price and a small plate thickness, it is possible to produce relatively cheap and effective cross-flow exchangers with the use of a thin steel plate. A similar conclusion regarding the material for the construction of counter flow exchangers is presented in [5].

It is worth highlighting that the remark mentioned in article [13] that "it is crucial that the material is as thin as possible" does not mean that the use of membrane plates in the exchanger is necessary. In the exchangers used in practice, the plates are relatively thick (approx. 1.2 mm). The presented conclusion mainly has the informative value that reducing the thickness of the steel plate by half leads to a reduction in the production costs of the exchanger, does not weaken its structure, as may happen with membrane plates, and the reduction in efficiency resulting from such a reduction in thickness is insignificant.

Exchanger operation time is significant to the temperature of air supplied to the room. In the case of cold periods, this time should be shorter. In the case of temperatures above 0 degrees, the exchanger operation time can be longer and the computation results indicate that 300 s is the best option.

Author Contributions: Conceptualization, K.G., A.M. and A.Ś.; methodology, K.G. and A.M.; software, A.M.; validation, K.G., A.M. and A.Ś.; formal analysis, K.G. and A.M.; investigation, K.G. and A.M.; resources, K.G., A.M. and A.Ś.; data curation, K.G., A.M. and A.Ś.; writing—original draft preparation, K.G.; writing—review and editing, K.G. and A.M.; visualization, K.G. and A.M.; supervision, K.G. and A.M.; project administration, K.G.; funding acquisition, K.G. and A.M. All authors have read and agreed to the published version of the manuscript.

Funding: Kielce University of Technology.

Institutional Review Board Statement: Not applicable.

Informed Consent Statement: Not applicable.

Data Availability Statement: Not applicable.

Conflicts of Interest: The authors declare no conflict of interest.

Nomenclature

Latin Symbols	
$a = \frac{k}{\rho c}$	thermal diffusivity coefficient, $\left[\frac{\mathrm{m}^2}{\mathrm{s}}\right]$
Bi	Biot number, compare (2)
c	for specific heat, [J/(kg K)]
Fo	Fourier number (dimensionless time), comp (2)
h	air duct height, [m]
k	thermal conductivity coefficient, [W/(mK)]
$l = 1.2$	plate section length, [m]
$Re = v_a h/\nu$	Reynolds number
T	temperature, [K],
$T_w = T(x, -1, z, t)$	
$T_c = T(-1, y, z)$	
$T_M^{ap}(x, y, z)$	approximation of temperature
$\overline{t}$	time, [s]
t	dimensionless time
v_a	velocity of air moving between plates, [m/s]
$\overline{x}, \overline{y}, \overline{z}$	spatial coordinates, [m]
$x,\ y,\ z$	dimensionless spatial coordinates
Greek Symbols	
$\alpha_1,\ \alpha_2$	heat transfer coefficients, [W/(m^{2}K)]
η_T	efficiency of the heat exchanger
ρ	density, [kg/m^3]
ν	kinematic viscosity, [mm^2/s]
∇	nabla operator,
$\nabla^2 \equiv \Delta$	Laplace operator

References

1. Shah, R.K.; Sekulic, D.P. Chapter 1, Classification of Heat Exchangers. In *Fundamentals of Heat Exchanger Design*; John WIley and Sons: Hoboken, NJ, USA, 2003; pp. 1–77.
2. Wang, L.; Sundén, B.; Manglik, R.M. *Plate Heat Exchangers, Design, Applications and Performance*; WIT Press Southampton: Boston, MA, USA, 2007.
3. Available online: https://www.rekuperatory.pl/rekuperator#co-to-jest-rekuperator (accessed on 31 June 2021).
4. Xu, K. Design and Optimization of Plate Heat Exchanger Networks. Ph.D. Thesis, The University of Manchester, Faculty of Science and Engineering, Manchester, UK, 2019.
5. Grysa, K.; Maciąg, A.; Ściana, A. Comparison of the Efficiency of Two Types of Heat Exchangers with Parallel Plates Made of Varied Materials. *Energies* **2021**, *14*, 8562. [CrossRef]
6. Available online: https://wentylacja.com.pl/news/plytowe-wymienniki-krzyzowe-do-odzysku-ciepla-63582.html (accessed on 8 July 2022).
7. Gao, T.; Sammakia, B.G.; Geer, J.F.; Ortega, A.; Schmidt, R. Dynamic Analysis of Cross Flow Heat Exchangers in Data Centers Using Transient Effectiveness Method. *IEEE Trans. Compon. Packag. Manuf. Technol.* **2014**, *4*, 1925–1935. [CrossRef]
8. Vali, A.; Simonson, C.J.; Besant, R.W.; Mahmood, G. Numerical model and effectiveness correlations for a run-around heat recovery system with combined counter and cross flow exchangers. *Int. J. Heat Mass Transf.* **2009**, *52*, 5827–5840. [CrossRef]
9. Vali, A.; Ge, G.-M.; Besant, R.W.; Simonson, C.J. Numerical modeling of fluid flow and coupled heat and mass transfer in a counter-cross-flow parallel-plate liquid-to-air membrane Energy exchanger. *Int. J. Heat Mass Transf.* **2015**, *89*, 1258–1276. [CrossRef]
10. Das, R.S.; Jain, S. Performance characteristics of cross-flow membrane contactors for liquid desiccant systems. *Appl. Energy* **2015**, *141*, 1–11. [CrossRef]
11. Shen, K.; Zhang, Z.-D.; Zhang, Z.-Q.; Yang, Y.-W. Investigation of effect on cross-flow heat exchanger with air flow non-uniformity under low Reynolds number. *Adv. Mech. Eng.* **2017**, *9*, 1687814017708088. [CrossRef]
12. Bai, H.-Y.; Zhu, J.; Chen, Z.-W.; Chu, J.-Z. Parametric analysis of a cross-flow membrane-based parallel-plate liquid desiccant dehumidification system: Numerical and experimental data. *Energy Build.* **2018**, *158*, 494–508. [CrossRef]

13. Dvořák, V.; Vít, T. Numerical investigation of counter flow plate heat exchanger. *Energy Procedia* **2015**, *83*, 341–349. [CrossRef]
14. Carslaw, H.S.; Jaeger, J.C. *Conduction of Heat in Solids*; Oxford University: Oxford, UK, 1959.
15. Mills, A.F. *Basic Heat and Mass Transfer*; Prentice-Hall: Upper Saddle River, NJ, USA, 1999.
16. Mills, A.F.; Coimbra, C.F.M. *Basic Heat and Mass Transfer*; Temporal Publishing, LLC: San Diego, CA, USA, 2015.
17. Available online: https://thermopedia.com/content/1187/ (accessed on 8 October 2022).
18. Available online: https://www.engineersedge.com/thermodynamics/overall_heat_transfer-table.htm (accessed on 9 September 2021).
19. Inhelder, J. Verbrauchs und Schadstoffoptimiertes Ottomotor-Aufladekonzept, ETH No. 11948. Ph.D. Thesis, Swiss Federal Institute of Technology, Zürich, Switzerland, 1996.
20. Eriksson, L.; Nielsen, L. *Modeling and Control of Engines and Drivelines*; Wiley: New York, NY, USA, 2014; p. 530.
21. Sforza, P. *Commercial Airplane Design Principles*; Elsevier Inc.: Amsterdam, The Netherlands, 2014; ISBN 978-0-12-419953-8.
22. White, F. *Fluid Mechanics*, 4th ed.; McGraw-Hill Higher Education: New York, NY, USA, 2002; ISBN 0-07-228192-8.
23. Incropera, F.P.; DeWitt, D.P. *Fundamentals of Heat Transfer*; Wiley: New York, NY, USA, 1981; ISBN 978-0-471-42711-7.
24. Trefftz, E. Ein Gegenstueck zum Ritz'schen Verfahren. In Proceedings of the 2nd International Congress of Applied Mechanics, Zurich, Switzerland, 12–17 September 1926; pp. 131–137.
25. Grysa, K.; Maciejewska, B. Trefftz functions for non-stationary problems. *J. Theoret. Appl. Mech.* **2013**, *50*, 251–264.
26. Frąckowiak, A.; Wróblewska, A.; Ciałkowski, M. Trefftz numerical functions for solving inverse heat conduction problems. *Int. J. Therm. Sci.* **2022**, *177*, 107566. [CrossRef]
27. Frąckowiak, A.; Ciałkowski, M.; Wróblewska, A. Iterative algorithms for solving inverse problems of heat conduction in multiply connected domains. *Int. J. Heat Mass Transf.* **2012**, *55*, 744–751. [CrossRef]
28. Ciałkowski, M.J.; Frackowiak, A. Thermal and related functions used in solving certain problems of mechanics, Part, I. Solving some differential equations with the use of inverse operator. In *Modern Problems of Technics*; University of Zielona Góra Publishers: Zielona Góra, Poland, 2003; Volume 3, pp. 7–70.
29. Maciąg, A.; Grysa, K. Trefftz Method of Solving a 1D Coupled Thermoelasticity Problem for One- and Two-Layered Media. *Energies* **2021**, *14*, 3637. [CrossRef]
30. Pudlik, W. *Exchange and Heat Exchangers*; Gdańsk University of Technology: Gdańsk, Poland, 2012; p. 320. Available online: https://pbc.gda.pl/Content/4404/wymiana-i-wymienniki-final.pdf (accessed on 8 July 2022). (In Polish)
31. Available online: https://www.engineeringtoolbox.com/heat-recovery-efficiency-d_201.html (accessed on 8 December 2021).
32. Available online: https://agmetalminer.com/metal-prices/ (accessed on 8 July 2022).
33. Available online: https://www.moneymetals.com/copper-prices (accessed on 8 July 2022).